THE ASTROPHYSICAL JOURNAL, 950:19 (11pp), 2023 June 10 https://doi.org/10.3847/1538-4357/acccf5

Near-core Acoustic Glitches Are Not Oscillatory: Consequences for Asteroseismic Probes of Convective Boundary Mixing

Christopher J. Lindsay[1], J. M. Joel Ong[2,3], and Sarbani Basu[1]
[1] Department of Astronomy, Yale University, P.O. Box 208101, New Haven, CT 06520-8101, USA; christopher.lindsay@yale.edu
[2] Institute for Astronomy, University of Hawai'i, 2680 Woodlawn Drive, Honolulu, HI 96822, USA
Received 2023 January 12; revised 2023 April 10; accepted 2023 April 12; published 2023 June 7

Abstract

Asteroseismology has been used extensively in recent years to study the interior structure and physical processes of main-sequence stars. We consider prospects for using pressure modes (p-modes) near the frequency of maximum oscillation power to probe the structure of the near-core layers of main-sequence stars with convective cores by constructing stellar model tracks. Within our mass range of interest, the inner turning point of p-modes as determined by the Jeffreys–Wentzel–Kramers–Brillouin (JWKB) approximation evolves in two distinct phases during the main sequence, implying a sudden loss of near-core sensitivity during the discontinuous transition between the two phases. However, we also employ non-JWKB asymptotic analysis to derive a contrasting set of expressions for the effects that these structural properties will have on the mode frequencies, which do not encode any such transition. We show analytically that a sufficiently near-core perturbation to the stellar structure results in nonoscillatory, degree-dependent perturbations to the star's oscillation mode frequencies, contrasting with the case of an outer glitch. We also demonstrate numerically that these near-core acoustic glitches exhibit strong angular degree dependence, even at low degree, agreeing with the non-JWKB analysis, rather than the degree-independent oscillations that emerge from JWKB analyses. These properties have important implications for using p-modes to study near-core mixing processes for intermediate-mass stars on the main sequence, as well as for the interpretation of near-center acoustic glitches in other astrophysical configurations, such as red giants.

Unified Astronomy Thesaurus concepts: Asteroseismology (73); Stellar physics (1621); Stellar evolution (1599); Main sequence (2047)

1. Introduction

The long temporal baselines of the Kepler (Borucki et al. 2010) and TESS (Ricker et al. 2015) missions make the interiors of thousands of stars amenable to examination through the asteroseismology of individual mode frequencies in their photometric power spectra. Stars with convective envelopes, such as our Sun, oscillate in multiple modes excited by convective motions (Goldreich & Keeley 1977a, 1977b). The frequencies of these oscillation modes can trace stellar structure in the deep interior, thereby encoding information about the star's evolutionary state (Chaplin & Miglio 2013; García & Ballot 2019, and references therein). The internal modes of solar-type oscillators are generally classified as either p-modes—where the restoring force is pressure—or g-modes—where the restoring force is gravity. Asymptotic analysis of wave propagation in stars under the Jeffreys–Wentzel–Kramers–Brillouin (JWKB) approximation (see Gough 2007) indicates that all nonradial modes are limited in their sensitivity to different regions of the star, depending on their character. In Sun-like stars, p-modes and g-modes occur in different regions: p-modes propagate in the outer convective envelope, and g-modes in the core. The loci of these different classes of modes are governed by two characteristic frequencies: the Lamb frequency

$$S_\ell^2 = \frac{\ell(\ell+1)c_s^2}{r^2}, \quad (1)$$

and the Brunt–Väisälä (or buoyancy) frequency

$$N^2 = -g\left(\frac{1}{\Gamma_1 P}\frac{dP}{dr} - \frac{1}{\rho}\frac{d\rho}{dr}\right); \quad (2)$$

where ℓ is the angular degree of the mode, c_s the sound speed, P the pressure, ρ the density, and r the radial coordinate. Waves that are higher in frequency than both these frequencies are p-modes (shaded in orange in Figure 2), while those that are lower in frequency than both are g-modes (shaded in blue). For stars on the main sequence, these p- and g-mode cavities are well separated both in frequency and spatially, so any normal modes with observable amplitudes (that is, with frequencies near that of maximum oscillation power, $\nu_{\max}$) are purely acoustic (p-modes). The depth to which p-modes sample the stellar structure is set by the Lamb frequency of the corresponding ℓ, which, due to its dependence on the sound speed, will also depend on the mean molecular weight gradient ∇_μ. Depending on the properties of near-core mixing, as well as how evolved the star is along the main sequence, the observed p-modes may therefore not penetrate deeply enough to reach the convective cores of main-sequence stars—thereby, in principle, limiting the applicability of these p-modes for diagnosing the nature of such near-core mixing, under the WKB approximation.

[3] Hubble Fellow.

The interior locations of convective boundaries and abundant element ionization zones are frequently studied through asteroseismic "glitch" analysis. Steep variations in the first adiabatic index, Γ_1, or in the sound speed, are known to introduce an oscillatory component ($\delta\nu$) to the frequencies of low angular degree stellar oscillation modes (e.g., Gough & Thompson 1988; Vorontsov 1988; Gough 1990; Basu et al. 1994). A number of investigations have explored the theoretical seismic consequences arising from sharp variations in the internal stellar structure at the convective envelope boundary (e.g., Monteiro et al. 2000) or in the region of helium ionization (Monteiro et al. 1998; Houdek & Gough 2007). These glitch signals are present across a range of stellar evolutionary states, and they have been used to investigate the properties of convection and ionization zones in both red giant stars (Miglio et al. 2010; Corsaro et al. 2015; Vrard et al. 2015; Dréau et al. 2020) and Sun-like main-sequence stars (Mazumdar et al. 2012, 2014). Because these convective envelope and helium ionization zone features are localized far outside the convective core, in this work we will refer to these glitches as "outer glitches."

The sharp variations in stellar structure present at the boundaries of convective cores are also expended to leave a signature on the oscillation frequencies of a star. However, any such signature from a convective core will have properties different than those generated from an outer glitch, owing to their localization close to the stellar center rather than the surface. Roxburgh & Vorontsov (2001) investigated the expected seismic signatures resulting from a glitch in the neighborhood of a convective core, provided that the structural variation was located well within the mode propagation cavity, far from the turning point of the oscillations. Similar analyses were performed by Provost et al. (1993) in the case of structural variations at the boundary of Jupiter's core and by Audard et al. (1995) in the case of intermediate mass (1.7–2.0 $M_\odot$) stars with g-mode pulsations. In the case of a lower-mass (1.2–1.5 $M_\odot$) main-sequence star, though, the aforementioned works do not apply, as the convective core is small, with its boundary located very close to the inner turning point of the oscillation modes.

Mazumdar et al. (2006) studied the seismic effects of small convective cores in stellar models and proposed a combination of small frequency separations with the goal of determining the presence of convective overshooting. A similar investigation was carried out by Cunha & Metcalfe (2007), who found that the seismic signatures of small convective cores are non-oscillatory and frequency-dependent. They suggest a combination of frequency separation ratios that may have diagnostic potential for studying convective cores in real stars with high-quality asteroseismic data. However, as with Mazumdar et al. (2006), their proposed diagnostic combined information from modes of different degrees. As such, they were unable to investigate the angular degree dependence of the seismic signal (instead assuming a priori that it would only affect the radial modes). Brandão et al. (2010) further investigated these diagnostics to look for age dependence. Cunha & Brandão (2011) built on the work of Cunha & Metcalfe (2007) and further investigated the seismic signatures of small convective cores. In particular, the work modeled the structural variation at the edge of convective cores in a more physically motivated fashion to study the evolution of their seismic diagnostic as a star advances in age.

In this work, we investigate the near-core locations available for study through low angular degree mode glitch signature analysis, both within (Section 2) and outside (Section 3) the WKB approximation, using evolutionary tracks of stellar models. We discuss our results and compare our work to previous studies of the seismic signatures of convective cores in Section 4.

2. WKB Analysis with Stellar Models

To illustrate the evolution of the well-mixed core and p-mode penetration depths, we construct stellar model tracks with masses between 1.2 and 1.5 $M_\odot$ using MESA version r12778 (Paxton et al. 2011, 2013, 2015, 2018, 2019). We construct models using an Eddington-gray atmospheric boundary condition and the mixing-length prescription of Cox & Giuli (1968). Elemental diffusion following the formulation of Thoul et al. (1994) was included with mass-dependent scaling (see Viani et al. 2018). We show results for three model tracks with $M = 1.2$, 1.4, and 1.5 $M_\odot$, calculated with solar-calibrated initial values of helium abundance ($Y_0 = 0.273$), metallicity (relative to Grevesse & Sauval 1998), and mixing length ($\alpha_{\rm mlt} = 1.81719$). MESA's implementation of overmixing (see Section 2 of Lindsay et al. 2022) from the convective core was also used, with $f_{ov} = 0.05$.

Within the WKB approximation, nonradial p-modes are assumed to only be sensitive to stellar structure within a mode cavity bounded on the inside by the WKB inner turning point, where the mode angular frequencies are equal to the Lamb frequency. For nonradial modes of the same frequency, this inner turning point's radius value increases with ℓ, and it is thus deepest for dipole modes. Accordingly, we show in Figure 1 the evolution of both the outer boundary of the well-mixed core, R_c, as well as of the inner turning points of dipole p-modes at $\nu_{\rm max}$, $R_{\ell=1}$, over the course of evolution along these tracks (parameterized by the central hydrogen fraction $X_{\rm H}$). We define R_c as the location where the chemical gradient ∇_μ changes by more than 0.1 between adjacent mesh points, while $R_{\ell=1}$ is the innermost point where $S_{\ell=1} = 2\pi\nu_{\rm max}$. Locations are indicated with respect to the relative mass coordinate $m(r)/M$.

From Figure 1, we see that, for the 1.4 and 1.5 $M_\odot$ evolutionary tracks (solid and dotted–dashed lines), $R_{\ell=1}$ begins increasing steadily with evolution along the main sequence. This steady rise is interrupted by a sharp discontinuity just after reaching $X_{\rm H} = 0.3$ for the 1.4 $M_\odot$ track and just before reaching $X_{\rm H} = 0.3$ for the 1.5 $M_\odot$ track. After this jump in $R_{\ell=1}$, the dipole p-mode inner turning point at $\nu_{\rm max}$ lies outside the near-core layers of these stars, rendering them insensitive to this region. Conversely, this discontinuous jump in $R_{\ell=1}$ does not occur in the 1.2 $M_\odot$ track because, given our specific combination of model input parameters, the position of the p-mode inner turning point starts (at zero age main sequence) at approximately the same location as the well-mixed core outer boundary ($R_{\ell=1} \approx R_c$). Therefore, for this example 1.2 $M_\odot$ track, nonradial modes may not be used (under the JWKB approximation) to probe the near-core layers, no matter how far along the main sequence the star has evolved.

These discontinuities in the evolution of the p-mode inner turning point ($R_{\ell=1}$) emerge from kinks in the Lamb frequency profile, caused by the change in mean molecular weight gradient at the boundary of the star's convective core. To examine the underlying mechanism for this, we show

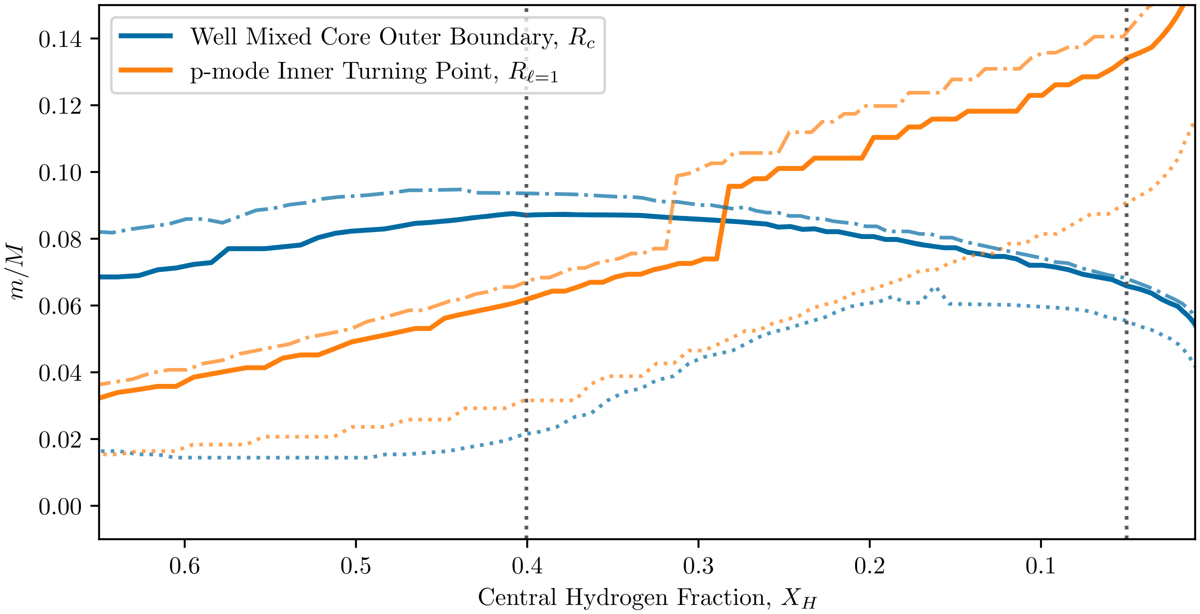

Figure 1. Evolution of the well-mixed core outer boundary (blue) inner turning point (orange) of $\ell = 1$ modes near $\nu_{\max}$ in mass coordinates for 1.2 $M_\odot$ (dotted), 1.4 $M_\odot$ (solid), and 1.5 $M_\odot$ (dotted–dashed) mass model tracks. Evolution goes from left to right as central hydrogen fraction decreases along the main sequence.

propagation diagrams from the 1.4 $M_\odot$ track, before and after this discontinuous jump in $R_{\ell=1}$, in Figure 2. The spikes in buoyancy frequency (N, solid black lines), which correspond to local enhancements of ∇_μ, coincide with localized kinks in Lamb frequency ($S_{\ell=1}$, dotted lines). As the star evolves, these kinks move inward, and the Lamb frequency at their location increases relative to $\nu_{\max}$ (horizontal dotted–dashed line). When these kinks coincide with $\nu_{\max}$, this results in a temporally discontinuous increase in $R_{\ell=1}$. Because the pulsation wave function is assumed to decay exponentially in the WKB-evanescent region, this corresponds to a discontinuous reduction in the probing power of dipole modes to these near-core features on either side of this evolutionary boundary.

Unlike the nonradial modes, the radial ($\ell = 0$) modes are known to penetrate more deeply into the stellar interior. These modes admit description by an equation of Schrödinger form (i.e., the "normal form" of Gough 2007, for JWKB analysis), with respect to the acoustic radial coordinate $t(r) = \int_0^r dr/c_s$, where the acoustic potential function V (shown in Figure 2), is set by the stellar structure and determines the behavior of their wave functions near the center (see, e.g., Gough 1993; Roxburgh 2010; Ong & Basu 2019, for a thorough discussion of the radial-mode acoustic potential). Localized enhancements in this potential function are known to yield oscillatory signatures (e.g., Houdek & Gough 2006), known colloquially as "glitches." Accordingly, we show this acoustic potential function in both propagation diagrams of Figure 2 (scaled by $\nu_{\max}$, using the gray dotted–dashed lines). Sharply localized peak-like features in V can be seen to emerge, corresponding to the locations in the star where chemical abundances vary rapidly with depth (near $m/M = 0.09$ and $m/M = 0.07$ for the $X_{\rm H} = 0.4$ and $X_{\rm H} = 0.05$ Figure 2 propagation diagrams, respectively). As such, these features must also have a direct effect on the radial-mode frequencies.

3. Beyond the WKB Approximation

Thus far, our discussion has taken place within the context of the commonly used WKB approximation (Gough 1993, 2007). This is qualitatively suitable where the acoustic glitches are situated far enough away from the turning points of the mode cavity that the behavior of the wave functions there may be treated as approximately sinusoidal. However, at the turning points, the solutions are instead more accurately approximated by Airy functions, which relate to these sinusoidal solutions through the asymptotic expansion of the Airy functions at large argument, by way of the Jeffreys connection formulae (i.e., the "J" of JWKB). In turn, the use of Airy functions near the turning points is only justifiable when boundary conditions of the pulsation problem as a whole can be neglected. The resulting oscillatory variations induced into the mode frequencies from such analysis (e.g., Houdek & Gough 2006) have historically been assumed to emerge even in existing theoretical studies of p-mode convective core signatures (e.g., Monteiro et al. 1998; Mazumdar & Antia 2001). However, the near-core structural discontinuities in the mass range under consideration here do not possess these properties. Because these features, as well as the turning points themselves, are localized close to the core, the inner boundary condition may no longer be neglected. Because the glitches may not be inside the WKB-oscillatory region as is typically assumed, the wave functions likewise may not be approximated well as sinusoidal there. As such, we must pursue an alternative derivation of the frequency perturbations induced by these glitch features accounting for these properties, which may correspondingly yield qualitatively different behavior from the standard sinusoidal phenomenology.

3.1. Analytic Development

From local asymptotic theory, it is known that the scaled p-mode radial Lagrangian displacement wave functions, $\psi = \xi_r \sqrt{\rho r^2 c_s}$, near the center of the star may be approximated by linear combinations of Riccati–Bessel functions of degree ℓ, with argument ωt. These linear combinations are in turn described well by using only the Bessel function of the first kind, with further position-dependent phases added to the argument. We refer the reader to Calogero (1963) and

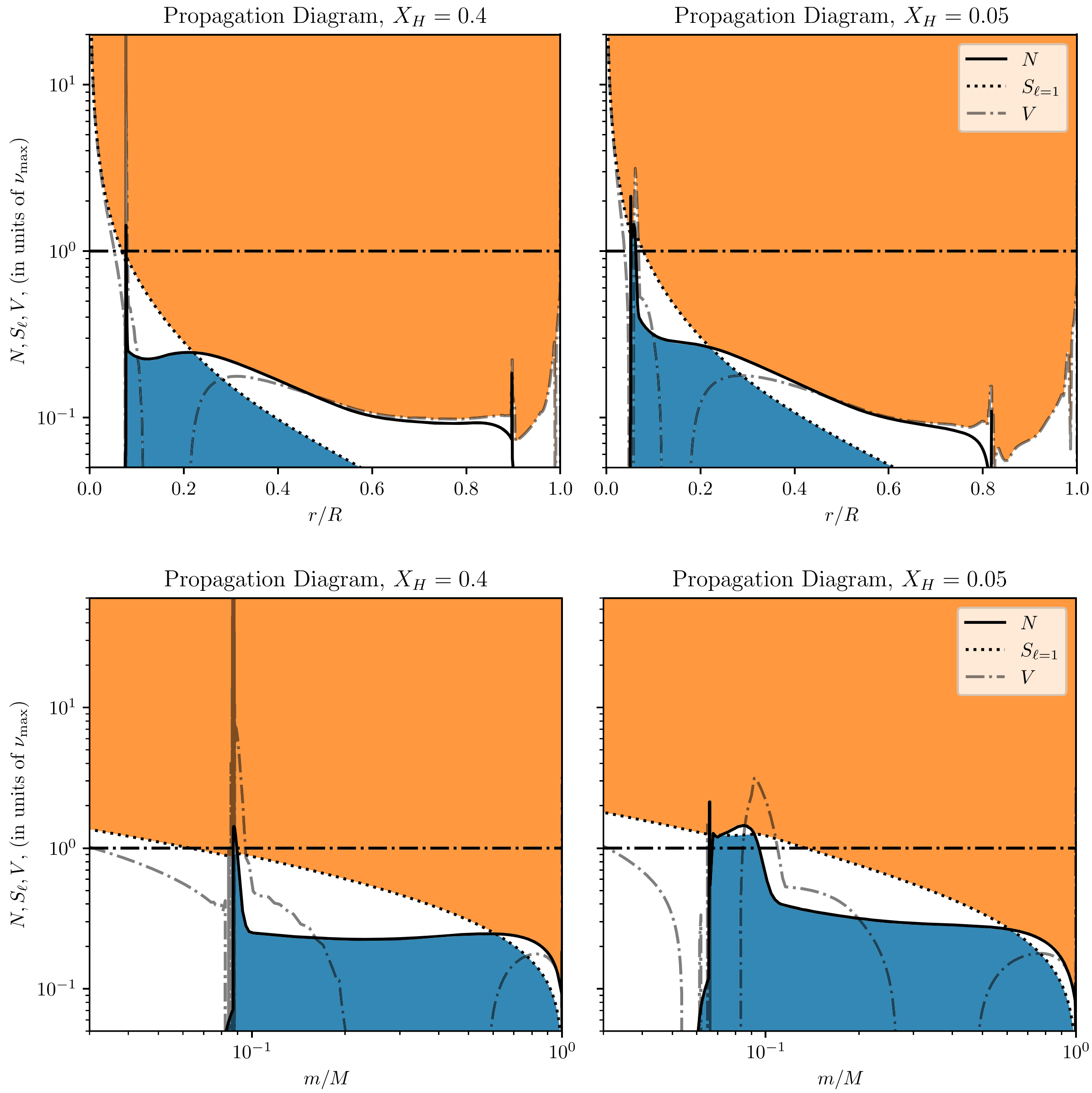

Figure 2. Upper Left Panel: Propagation diagram for a 1.4 $M_\odot$ model with $X_H = 0.4$ (leftmost vertical gray dotted line in Figure 1) showing, in units of $\nu_{\max}$, the buoyancy frequency (N), the Lamb frequency ($S_{\ell=1}$), and the acoustic potential, V, which is a characteristic frequency describing the propagation of a star's radial modes. The orange region of the propagation diagrams represent the regions where p-modes can propagate, while the blue regions represent the g-mode propagation regions. In the outer layers of the star, the minimum frequency at which p-modes can propagate is governed by the critical frequency ($\nu_{\rm crit}$ mirrors V near the model's surface) in the outer layers. Upper Right Panel: Same as the left panel, but for the 1.4 $M_\odot$ model later in evolution (right gray dotted line in Figure 1, $X_H = 0.05$). Lower Panels: Propagation diagrams for the same two models as in the upper panels, but the x-axis shows the relative mass coordinate in log-scale in order to show the near-core features in more detail. The acoustic potential, V, shows a sharp, localized peak at the position of the near-core glitch.

Babikov (1976) for more details about this construction, and to Roxburgh (2010) and Ong & Basu (2019) for more detailed discussion of the use of such phase functions in the context of p-modes. Here, we use $s_\ell(x) = x j_\ell(x)$ to refer to the Riccati–Bessel functions of degree ℓ of the first kind, rather than the customary S_ℓ, to avoid confusion with the Lamb frequency.

We first consider sharp variations in the Brunt–Väisälä frequency relative to a smooth background, $N^2 = N^2_{\rm smooth} + \delta N^2$, and wave functions that are unit normalized under the usual inner product. These sharp variations exist in our stellar models (see the N profiles in Figure 2) and are collocated with enhancements to the acoustic potential V, which encapsulates all the relevant information for radial modes. By inspection of the wave equations (e.g., Ong & Basu 2020, and also Appendix B), δN^2 induces deviations in the mode frequencies, ceteris paribus, as

$$\delta(\omega^2) \sim \int \xi_r^2 \cdot \delta N^2 \, dm, \tag{3}$$

compared to if only $N_{\rm smooth}$ were present, to leading order in perturbation theory (as also used in, e.g., Houdek & Gough 2006, 2007). We first recount how the usual expression of these glitches, relating δ-function features in the Brunt–Väisälä frequency, $\delta N^2 \sim \delta(r - r_0)$, to sinusoidal perturbations to the mode frequencies, may be recovered from this description. Near the outer boundary, $t = T$, the glitch signature of such a δ-function feature may be computed with an approximate expression for the outer phase function of the form

$$\delta(\omega^2) \sim \omega\delta\omega \sim \int dm\ \xi_r^2 \delta(r - r_0) \sim \int dt\ \psi^2(t)\ \delta(t - t_0)$$
$$\sim s_\ell^2\left(\omega t_0 - \alpha_\ell(\omega, T - t_0) + \pi\left(n_p + \frac{\ell}{2}\right) - \omega T\right), \quad (4)$$

where r_0 and t_0 are the physical and acoustic radii of the localized feature, n_p is the radial order of the mode, and α_ℓ is the phase function induced by the outer boundary condition. Far away from the center, the star may be approximated well as being plane-parallel-stratified, and so the outer phase functions α_ℓ do not materially depend on ℓ at low degree (e.g., Roxburgh 2016). The usual expression for acoustic glitches—i.e., $\delta\omega \sim \sin[2\omega(T - t_0) + \phi]$ for all ℓ, up to some frequency-dependent amplitude function—is then recovered upon introducing the asymptotic expansion of Riccati–Bessel functions as sinusoids at large argument: $s_l(x) \sim \sin\left(x - \pi\frac{\ell}{2}\right) + \mathcal{O}(1/x)$.

However, as we have described above, this usual derivation does not apply to these core acoustic glitches. Rather, because the glitches we consider are localized near the center of the star, we must instead make use of the converse expansion of Riccati–Bessel functions as power laws at small argument (see Arfken & Weber 2005, and Appendix A):

$$s_l(x) \sim \frac{x^{\ell+1}}{(2\ell+1)!!}, \quad \text{where } |x| \ll \sqrt{\ell + \frac{3}{2}}, \quad (5)$$

with the double exclamation marks denoting the semifactorial. Accordingly, the frequency perturbation induced by such near-core features takes the form

$$\delta\omega \sim \left(\frac{[\omega t_0 - \delta_\ell(\omega, t_0)]^{\ell+1}}{(2\ell+1)!!}\right)^2, \quad (6)$$

where $\delta_\ell(\omega, t)$ is an inner phase function induced by the inner boundary condition, satisfying $\delta_\ell(\omega, t) \to 0$ as $t \to 0$ under regular boundary conditions at the center (see Roxburgh 2010, 2016, although we note that, by using Riccati–Bessel functions here rather than sinusoids as in those works, we absorb the phase lag of $\pi\ell/2$ shown there—see Appendix A). This quantity can be seen to depend on ℓ. Qualitatively, this implies that any frequency perturbation induced by a near-center feature must (1) diverge gradually with increasing frequency (as opposed to being sinusoidal, like outer glitches), and (2) possess an amplitude that decreases rapidly with increasing ℓ (as opposed to the ℓ-independent behavior of outer glitches). In particular, because the semifactorial suppression with increasing ℓ is so steep, this effectively produces an offset of the radial-mode frequencies relative to all other ℓ.

The variations to the Brunt–Väisälä frequency profile by themselves do not account completely for all structural variations at the boundary. For example, there are also variations to the sound speed profile at the convective core boundary (seismic properties of which have been studied by, e.g., Mazumdar et al. 2006; Cunha & Metcalfe 2007; Cunha & Brandão 2011), which could dominate the glitch signature for radial modes. In this work, we restrict our analysis to only a deviation in the Brunt–Väisälä frequency profile, as we are interested in the qualitative properties of the near-core glitch signatures, namely their apparent nonoscillatory nature and strong dependence on angular degree, ℓ. As demonstrated in Figure 2, the sharp Brunt–Väisälä frequency features are collocated with enhancements to the acoustic potential, V, which also carries information about sound speed discontinuities.

Analyses similar to the one done for the Brunt–Väisälä frequency, applied to the sound speed or other structural properties, will yield the same strong-degree-dependence behavior in the frequency perturbations. More precise statements concerning the exact frequency dependence and amplitudes of the mode frequency differences would require an analysis similar to Cunha & Metcalfe (2007), incorporating structurally self-consistent perturbations to the relevant acoustic potentials. Perturbations to different quantities may yield different power-law indices in the frequency that may differ from that attributed to the Brunt–Väisälä frequency (if derivatives or integrals of the wave functions enter into the analogous kernel expressions to Equation (3)), while those caused by different features will have the arguments of their power laws be evaluated at different acoustic depths. Thus, the overall frequency perturbation that we would expect from these near-core features will take the form of a sum of various power-law terms. However, we note that the argument and overall amplitude of any one of these power-law terms are, in effect, entirely degenerate. Thus, an unprivileged observer, given a combination of power-law components resulting from near-core perturbations to the stellar structure, will find it mathematically impossible to distinguish the inner glitch depth from its amplitude.

3.2. Empirical Diagnostics

In the absence of a more quantitative description of the frequency dependence of the near-core glitch signatures, we can illustrate the qualitative properties of these near-core glitch signatures by computing the mode frequencies for each stellar model along our 1.2 $M_\odot$, 1.3 $M_\odot$, 1.4 $M_\odot$, and 1.5 $M_\odot$ tracks using the stellar oscillation code GYRE (version 6.0, Townsend & Teitler 2013). We calculate the radial ($\ell = 0$) as well as nonradial ($\ell = 1$, 2, and 3) mode frequencies in a wide frequency range, from a lower bound of $\Delta\nu$ up to $2\nu_{\max}$. We use scaling relations to approximate the global asteroseismic parameters of our stellar models based on the models' mass, radius, and temperature (see Kjeldsen & Bedding 1995), setting $\nu_{\max} = \nu_{\max,\odot} M/(R^2\sqrt{T_{\rm eff}})$ and $\Delta\nu = \Delta\nu_\odot\sqrt{M/R^3}$ where M, R, and $T_{\rm eff}$ are in solar units.

In order to enhance the visibility of these glitch signatures (oscillatory or otherwise), we take the second differences of the mode frequencies with respect to the modes' radial order n_p ($\delta^2\nu_{n,\ell}$; see Gough 1990; Basu et al. 1994, 2004; Mazumdar 2005; Verma et al. 2014), given by

$$\delta^2\nu_{n,\ell} = \nu_{n-1,\ell} - 2\nu_{n,l} + \nu_{n+1,\ell}. \quad (7)$$

For illustration, we show these second differences in the top panels of Figure 3 for the same two 1.4 $M_\odot$ models as in Figure 2 (before and after the discontinuous jump in the position of the p-mode inner turning point). As discussed previously, these can be seen to be dominated, for all ℓ shown, by the oscillatory variability of the outer ionization zone/convective boundary glitches, which should affect all ℓ equally, at least at these low

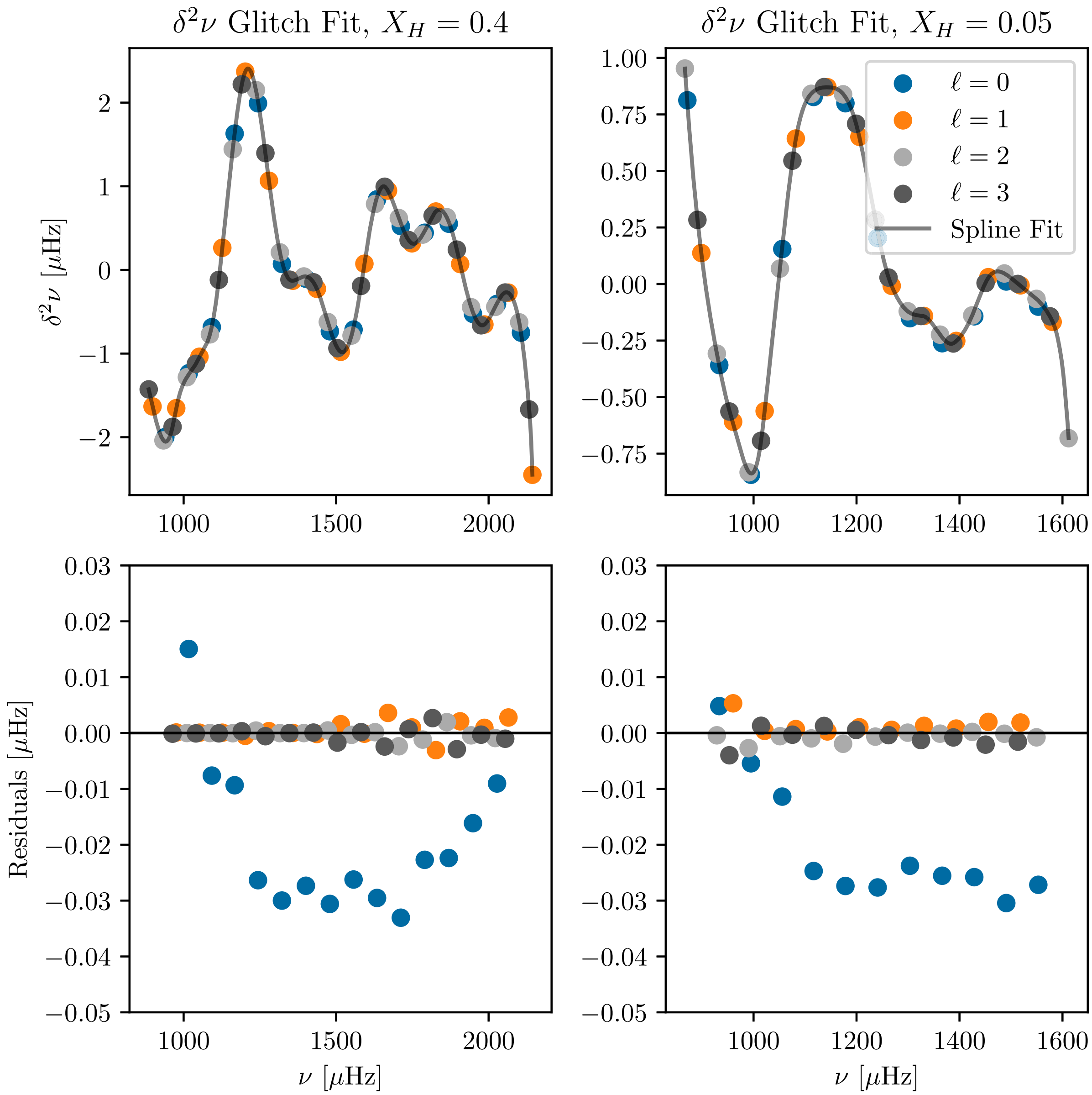

Figure 3. Top Panels: Plot of the second differences of the oscillation mode frequencies as a function of mode frequency for the same two 1.4 $M_\odot$ models as in Figure 2. The frequency ranges between 800 μHz up to the acoustic cutoff frequency of the model ($\nu_{\rm ac} = \frac{1}{2\pi}\frac{c_s g \rho}{P}$) where the sound speed (c_s), density (ρ), and pressure (P) are taken at the model surface (outermost grid point). The second differences are taken for each set of $\ell = 0$, 1, 2, or 3 modes with respect to the radial order n_p. The gray line shows a spline fit through the $\ell = 1$, 2, and 3 modes. Bottom Panels: Corresponding residuals (second differences minus the spline fit) as a function of frequency.

degrees. We thus fit this overall oscillatory signal in the second differences using a cubic spline, incorporating only second differences of the $\ell = 1$, 2, and 3 modes, as shown in the top panels of Figure 3 as gray lines. We show the residuals to this fit in the bottom panels of Figure 3. The residuals are such that the $\ell = 0$ mode are clearly systematically offset from the nonradial mode frequencies. Thus, our analytic prediction for the amplitude of the glitch signature decreasing with increasing angular degree (Equation (6)) is borne out numerically. We note that this systematic dependence of the residuals on ℓ stays consistent between different choices for how the outer glitches are detrended (e.g., fitting a high-order polynomial instead of a spline, or also including $\ell = 0$ modes in the fit). Moreover, no obvious qualitative difference between the two stellar models can be seen, despite their being in different JWKB regimes (as described earlier).

To investigate the amplitude of the near-core glitch over the course of the main-sequence evolution of our models, we computed the average second-frequency-difference residuals for each ℓ after subtracting a high-order polynomial fitted against $\delta^2\nu$ for $\ell = 0$, 1, 2, 3. For our 1.4 $M_\odot$ model track, we plot this average residual as a function of the center hydrogen fraction for each value of ℓ in the left panel of Figure 4. Overall, the amplitude of the $\ell = 0$ residuals is much larger than for the nonradial orders, agreeing with the analytic prediction that the amplitude of the frequency differences caused by the near-core glitch will decrease with increasing ℓ (Equation (6)). The right panel of Figure 4 shows the evolution of the average $\ell = 0$ residuals for our 1.3, 1.4, and 1.5 $M_\odot$ model tracks. These appear very similar for the 1.4 and 1.5 $M_\odot$ tracks, and they remain approximately constant over the course of their main-sequence evolution.

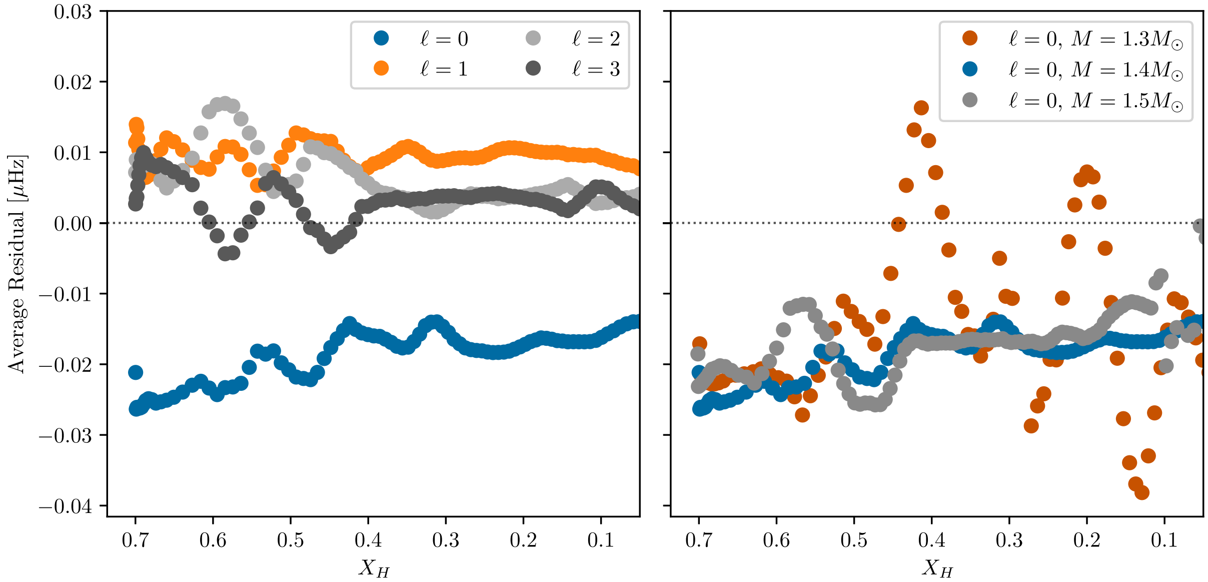

Figure 4. Left Panel: The evolution of the 1.4 $M_\odot$ model track's average second-frequency-difference residuals left over after subtracting a high-order polynomial fit from the $\ell = 0$, 1, 2, and 3 values of $\delta^2\nu$. The evolution is shown as a function of the central hydrogen fraction, $X_{\rm H}$. Right Panel: The evolution of the $\ell = 0$ values of average $\delta^2\nu$ residuals as a function of $X_{\rm H}$ for our 1.3, 1.4, and 1.5 $M_\odot$ tracks. Each curve is smoothed with a boxcar kernel with a size of five points.

Our procedure for isolating the near-core glitch's affect on the second-difference residuals results in the radial-mode residuals containing, but not necessarily completely isolating, the near-core glitch signal. For example, for much of the main sequence, the average $\ell = 0$, $\delta^2\nu$ residual amplitudes for the 1.3 $M_\odot$ track are overall smaller when compared with the residual amplitudes for the 1.4 and 1.5 $M_\odot$ tracks, in keeping with the smaller size of the 1.3 $M_\odot$ models' convective cores. While the 1.3 $M_\odot$ track residuals may be seen to vary much more significantly after passing $X_{\rm H} \approx 0.4$, this is not a feature of the near-core glitch, but rather a property of the outer glitches contaminating the second-difference residual signal. In particular, the convective envelope boundary of the 1.3 $M_\odot$ models is much deeper (in relative acoustic depth) compared with those of the 1.4 and 1.5 $M_\odot$ models. At around $X_{\rm H} \approx 0.4$, the acoustic depth of the 1.3 $M_\odot$ model's convective envelope boundary increases past $\tau = T/2$ (where T is the acoustic radius of the star). Interior to this, the glitch modulations affect not only the degree-independent outer phase function α_ℓ, but also the degree-dependent inner phase functions δ_ℓ (see Figure 5 of Roxburgh 2010); thus, the outer glitch may itself no longer be simply described as a function of frequency alone. As such, in this regime, the radial-mode residuals from such a fit will also contain contributions originating from the outer glitch, and they no longer serve to describe the near-core glitch well. Thus, we cannot guarantee that this method necessarily uniquely isolates the near-core glitch signal.

Cunha & Metcalfe (2007) have previously proposed an alternative means of eliminating the outer phase function by way of scaled separation ratios:

$$\frac{D_{0,2}}{\Delta\nu_{n-1,1}} - \frac{D_{1,3}}{\Delta\nu_{n,0}}, \tag{8}$$

where

$$D_{\ell,\ell+2} \equiv \frac{\nu_{n,\ell} - \nu_{n-1,\ell+2}}{4\ell + 6} \tag{9}$$

and

$$\Delta\nu_{n,\ell} \equiv \nu_{n+1,\ell} - \nu_{n,\ell}. \tag{10}$$

The unscaled separation ratios ($r_{\ell,\ell+2} = d_{\ell,\ell+2}/\Delta\nu_{n,\ell}$), considered as a function of frequency, were shown by Roxburgh (2005) to be approximated well by differences of the interior phase functions, $\delta_{\ell+2}(\nu) - \delta_\ell(\nu)$. The difference of the scaled ratios in Equation (8), which is the diagnostic of Cunha & Metcalfe (2007), is thus equivalent to taking a linear combination of the inner phase functions δ_0, δ_1, δ_2, δ_3, evaluated at some notional inner matching point, which is usually left underspecified. By contrast, in separating the acoustic depth from the inner phase function, we evaluate the inner phase function at the acoustic depth of the inner glitch. A further, subtle difference between these inner phase functions δ_ℓ appearing here and in our expressions is that those we consider above are of the "smooth" structure: they are therefore completely uninformative regarding the inner glitches, with all information about them contained instead in the ωt_0 term and the implicit constant of proportionality. By contrast, the δ_ℓ of the procedure of Cunha & Metcalfe (2007) are associated with the actual mode frequencies, including the near-core glitches. These differences render these two diagnostics not immediately quantitatively commensurate to each other, and deriving an explicit relationship between their diagnostic and ours lies beyond the scope of this work; at best, we will be able to perform only a qualitative comparison.

Plotting the diagnostic from Equation (8) as a function of frequency (Figure 5(a)) for three 1.4$M_\odot$ stellar models of different ages shows that this diagnostic, calculated for our model frequencies, shows properties similar to those shown Cunha & Metcalfe (2007), despite differences in the modeling physics and global stellar properties. Comparing the residuals of our outer glitch subtracting procedure (from Figure 3) for the same three models (shown in Figure 5(b)) with the diagnostic curves in Figure 5(a) shows the curvature is reversed between

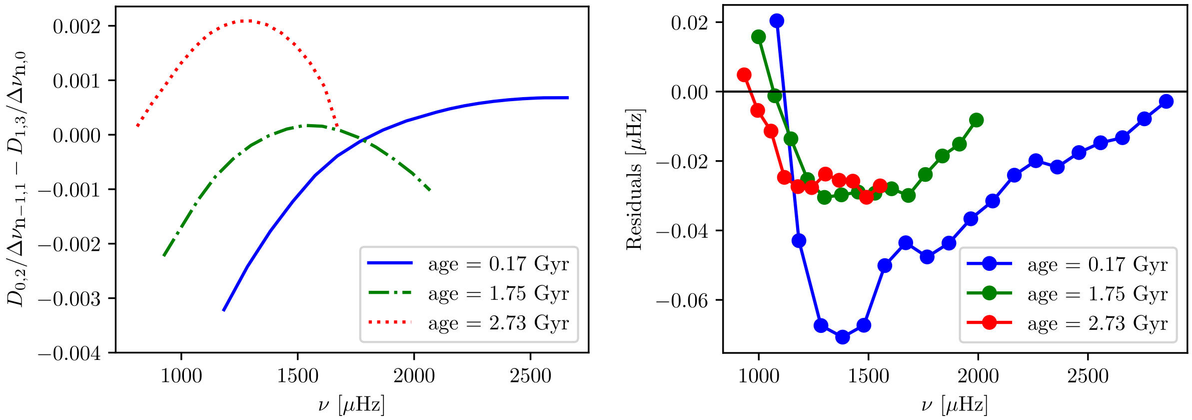

Figure 5. Left Panel: Frequency differences diagnostic defined by Equation (8) as a function of frequency for three $1.4M_\odot$ models at different ages. The model represented with the red dotted curve is the same as the model shown in the right panels of Figure 3. The model modes considered in this figure range in radial order from $n = 8$ to $n = 28$. Right Panel: The second-difference ($\delta^2\nu$) residuals obtained after subtracting the outer glitch signature from just the radial-mode values of $\delta^2\nu$, as a function of frequency. The curves are shown for the same three models shown in the left panel.

the two methods of displaying the inner, near-core glitch signal. However, both methods show that subtracting the outer glitches is necessary to reveal the small-amplitude seismic signatures of the convective cores. In addition, both panels of Figure 5 show that both methods of isolating the seismic signal of the near-core glitch on the radial modes reveals that these signals are age-dependent, meaning their glitch signature shape changes as a main-sequence star evolves on the main sequence.

Practically speaking, an operational difference between the diagnostic in Equation (8) and our method of subtracting a spline fit from the nonradial modes detailed in Section 3 is that octopole ($\ell = 3$) modes are not explicitly required by our construction. In principle, our proposed methodology accommodates data sets containing both fewer and more degrees than $\ell \in \{0, 1, 2, 3\}$. However, retrieving the asteroseismic signal of the convective cores would still be difficult unless many nonradial mode frequencies are available.

4. Discussion and Conclusion

Our analysis shows two distinct WKB regimes for the solar-like oscillators in question. Throughout the first regime, before the discontinuous increase in $R_{\ell=1}$, the realm that nonradial p-mode oscillations probe includes the near-core regions of the star, which is of particular importance for studies of convective boundary mixing processes like convective overshoot. During the second regime, after the sharp increase in $R_{\ell=1}$, the near-core layers around the stellar core are no longer accessible to nonradial p-mode oscillations with frequencies near $\nu_{\max}$. This suggested that the usefulness of these modes to study core processes in main-sequence stars would depend on the exact evolutionary history of that particular object, due to the sharp boundary between the two regimes. Acoustic glitch fitting is often used to determine the locations of particular stellar layers of interest, such as the boundaries of convection zones and the locations of ionization zones. In the first regime we discuss, where the p-mode outer turning point is exterior to the boundary of the well-mixed core, acoustic glitch fitting would be used to study the different layers of the star down past the boundary of the well-mixed core. In this case, glitch signatures from the boundary of the convective core will impart perturbations to the (near-$\nu_{\max}$) frequencies of both the radial and nonradial oscillation modes of the star. On the other hand, assuming the WKB approximation holds, after the discontinuous jump in $R_{\ell=1}$, the near-core glitch signature from the core convection zone boundary should be inaccessible to acoustic glitch analysis.

However, because the well-mixed convective core boundary exists sufficiently close to the center of the star such that the inner boundary condition can no longer be neglected, and R_c may not be inside the WKB-oscillatory region in any case, the glitch signature pattern from the core boundary imprints instead an ℓ-dependent signal onto the frequencies of the stellar oscillation modes. We demonstrate this behavior in Figure 3; after fitting out the dominant acoustic glitch signature from the $\ell = 0$, 1, 2, and 3 modes, an additional glitch signature is visible in the radial-mode residuals in both cases, which in neither case appears oscillatory. The results of this procedure can be seen to qualitatively resemble those obtained from other prior proposed diagnostics, such as that of Cunha & Metcalfe (2007) (Figure 5).

In contrast to the oscillatory and degree-independent nature of acoustic glitches in the outer parts of the star, we would therefore expect observationally to ultimately obtain, from isolating the inner glitch signal, some combination of nonoscillatory components, each exhibiting some power-law nature and strong angular degree dependence in their frequency perturbations. Crucially for the outer glitches, it is precisely their sinusoidal form that permits different components, localized at and attributed to different physical features, to be separately identified and characterized through their modulation frequency and amplitude (Monteiro et al. 1998; Mazumdar & Antia 2001; Houdek & Gough 2006). By contrast, because the amplitude and argument of a power law are mathematically indistinguishable, it is impossible to distinguish the amplitude of the inner glitch from its argument (i.e., location, via acoustic depth), let alone disentangle and assign interpretations to such linear combinations of them as we should expect to obtain in practice, without the imposition of further constraints from stellar modeling. Thus, our key qualitative result in this work—that inner glitches hold to power-law parameterizations—also indicates that any quantitative signal, however isolated observationally, will not be amenable to interpretation as easily as those derived from the outer glitches. Unfortunately, this means that any insights into the nature of near-core convective boundary mixing must necessarily derive from explicit reference to numerical models of stellar structure, unlike the model-independent diagnostic quantities returned from the outer glitches.

We note that the aforementioned near-core glitch properties we discuss in this work are only applicable to stars that are massive enough to host convective cores, but with low enough masses to have significant convective envelopes that drive p-mode oscillations. Therefore, future searches for seismic signatures of main-sequence small convective cores will need to limit their consideration to stars within a narrow mass range with good asteroseismic data.

Stellar structures like those discussed in this paper, characterized by steep, localized variations in structure near their cores, are not just present in intermediate-mass main-sequence stars. As low- and intermediate-mass stars run out of hydrogen in their cores and begin to evolve across the subgiant branch and up the red giant branch, their convective envelopes expand while their cores contract (see Hekker & Christensen-Dalsgaard 2017). At this stage of evolution, the interior boundary of the convective envelope reaches far into the core of the giant star, depending on the amount of envelope overshooting (see Section 4, Figure 4 of Lindsay et al. 2022). The steep variation in sound speed at the interior boundary of the envelope convection zone will induce a glitch component to the mode frequencies of the giant star, and because the location of the glitch would be near the core in this case, an ℓ-dependent signature similar to that described in Section 3 will be likewise present in the notional p-modes of these giants. Because the observable modes in red giant stars are, in practice, modes of mixed g- and p-like character, disentangling the deep envelope convection zone glitch signature from the overall mixed mode pattern of observed red giant oscillation modes would be challenging—but rewarding. Such constraints on the location of the envelope convective boundaries would define the correct amount of envelope overshooting, which should be incorporated into evolved star stellar models. These would be complementary to other constraints from "buoyancy" glitches, derived from the g-mode cavity (e.g., Cunha et al. 2019; Vrard et al. 2022). At the same time, the considerations we outline here may be required to interpret such buoyancy glitches: should they be localized near the g-mode turning points (as we describe in Lindsay et al. 2022), the relevant wave functions should be described with Airy functions of the first kind, as also used in Cunha & Metcalfe (2007), which would yield different behavior from the sinusoids considered in Cunha et al. (2019).

C.J.L. acknowledges support from a Gruber Science Fellowship. J.O. acknowledges support from NASA through the NASA Hubble Fellowship grant HST-HF2-51517.001 awarded by the Space Telescope Science Institute, which is operated by the Association of Universities for Research in Astronomy, Incorporated, under NASA contract NAS5-26555. S.B. acknowledges NSF grant AST-2205026. We also thank Dan Hey, Marc Hon, and the anonymous referee for their useful and constructive discussion, as well as the Yale Center for Research Computing for guidance and use of the research computing infrastructure.

Software: MESA (Paxton et al. 2011, 2013, 2015, 2018, 2019), GYRE (Townsend & Teitler 2013), SciPy (Virtanen et al. 2020), Pandas (Reback et al. 2021).

The MESA and GYRE inlists we used to generate our models and frequencies, as well as the resulting MESA models and frequencies, are archived on Zenodo and can be downloaded at doi:10.5281/zenodo.7705648.

Appendix A
Spherical Bessel Functions

The usual expression for the mode frequency shifts resulting from an acoustic glitch has the form $\delta\omega \sim \sin[2\omega(T - t_0) + \phi]$. However, in the case where the acoustic glitch is located sufficiently close to the real (coordinate) singularity at the center of the star, the usual expression for acoustic glitches does not apply. In Section 3, we made use of the converse expansion of Riccati–Bessel functions as power laws at small argument. Here, we expand on this discussion of spherical Bessel functions, drawing extensively from Section 11.7 of Arfken & Weber (2005).

Upon separation of variables of the wave equation, the radial wave function R satisfies an ordinary differential equation that is approximated well near the center of the star by an expression of the form

$$x^2\frac{d^2R}{dx^2} + 2x\frac{dR}{dx} \sim -[x^2 - \ell(\ell + 1)]R, \tag{A1}$$

where $\ell(\ell+1)$ is the separation constant from the angular components (ℓ is a non-negative integer) and the dimensionless argument $x \sim k_r r$ enters from the coordinate transformation required to put the original Helmholtz equation into this form. If one makes the substitution $R(x) = \frac{Z(x)}{\sqrt{x}}$, the radial equation becomes

$$x^2\frac{d^2Z}{dx^2} + x\frac{dZ}{dx} + \left[x^2 - \left(\ell + \frac{1}{2}\right)^2\right]Z = 0, \tag{A2}$$

which is Bessel's equation with Z being a Bessel function of order $\ell + \frac{1}{2}$. Defining

$$j_\ell(x) = \frac{s_\ell(x)}{x} = \sqrt{\frac{\pi}{2x}}J_{\ell+1/2}(x) \tag{A3}$$

and expressing J_ℓ as a series (see Section 11.1 of Arfken & Weber 2005):

$$\begin{aligned} J_{\ell+1/2}(x) &= \sum_{s=0}^{\infty}\frac{(-1)^s}{s!(s+\ell+\frac{1}{2})}\left(\frac{x}{2}\right)^{2s+\ell+\frac{1}{2}} \\ &= \frac{x^\ell}{2^\ell \ell!} - \frac{x^{\ell+2}}{2^{\ell+2}(\ell+1)!} + \ldots \end{aligned} \tag{A4}$$

we apply the Legendre duplication formula, $z!\left(z + \frac{1}{2}\right)! = 2^{-2z-1}\sqrt{\pi}(2z+1)!$, to each term. Thus, we have a series form for $j_\ell(x)$,

$$\begin{aligned} j_\ell(x) &= \sqrt{\frac{\pi}{2x}}\sum_{s=0}^{\infty}\frac{(-1)^s 2^{2s+2\ell+1}(s+\ell)!}{\sqrt{\pi}(2s+2\ell+1)!s!}\left(\frac{x}{2}\right)^{2s+\ell+\frac{1}{2}} \\ &= 2^\ell x^\ell \sum_{s=0}^{\infty}\frac{(-1)^s}{s!(2s+2\ell+1)!}x^{2s}. \end{aligned} \tag{A5}$$

Now in the limit of small argument, where $x \ll 2\sqrt{\frac{(2\ell+2)(2\ell+3)}{(\ell+1)}}$, we have

$$j_\ell(x) \approx \frac{2^\ell \ell!}{(2\ell+1)!}x^\ell = \frac{x^\ell}{(2\ell+1)!!}. \tag{A6}$$

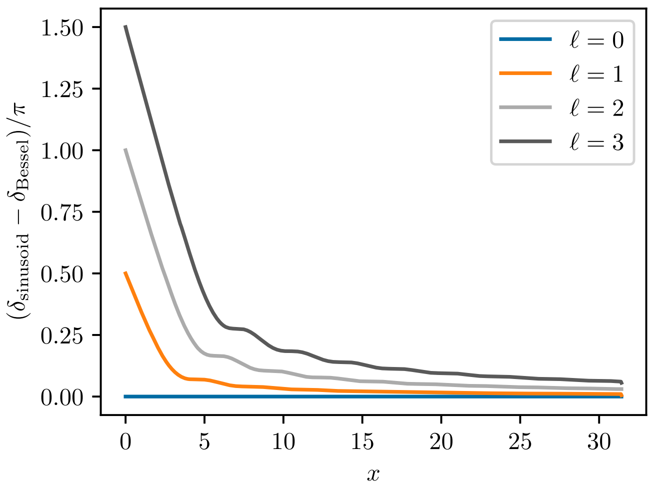

Figure 6. The inner phase function δ required to approximate a Riccati–Bessel function using a sinusoid.

The expressions in Section 3 are then recovered with argument $x = \omega t_0 - \delta_\ell(\omega, t_0)$.

Our use of the Riccati–Bessel functions here requires also that our inner boundary condition for δ differs from that of Roxburgh (2010, 2016), who use a sinusoidal approximation, such that the phase function required to approximate a wave function ψ with a sinusoid as $A \sin(\omega t + \delta)$ can be found as $\delta \sim \arctan\left(\psi \middle/ \frac{d\psi}{d(\omega t)}\right) - \omega t$. For illustration, we show this in Figure 6 for Riccati–Bessel functions s_ℓ of various degree. This is known to yield an offset of $\ell\pi/2$ in the argument as $t \to 0$, which is exactly equal to the inner boundary condition of Roxburgh (2010, 2016). Thus, $\delta_\ell \to 0$ as $t \to 0$ for all ℓ in our description, for consistency with these works further into the stellar interior.

Appendix B
Deviations to the Mode Frequencies

The displacement eigenfunctions $\boldsymbol{\xi}$ of normal modes with angular frequency ω satisfy the constraint

$$-\rho\omega^2\boldsymbol{\xi} = -\nabla P' + \boldsymbol{g}\rho' + \rho\nabla\Phi', \tag{B1}$$

where P', ρ', and Φ' are the accompanying eigenfunctions in the pressure, density, and gravitational potential perturbations for that mode. These other eigenfunctions may be eliminated with the use of other physical constraint equations to yield an operator eigenvalue equation, customarily written in the manifestly Hermitian form

$$\begin{aligned}-\rho\omega^2\boldsymbol{\xi} &= \nabla(\boldsymbol{\xi}\cdot\nabla P + c_s^2\rho\nabla\cdot\boldsymbol{\xi}) - \boldsymbol{g}\nabla\cdot(\rho\boldsymbol{\xi}) \\ &\quad - \rho G\nabla\left(\int d^3x' \frac{\nabla\cdot(\rho\boldsymbol{\xi})}{|x - x'|}\right) \\ &\equiv \rho\hat{\mathcal{L}}\boldsymbol{\xi}.\end{aligned} \tag{B2}$$

Small (and necessarily Hermitian) perturbations to the wave operator, of the form $\hat{\mathcal{L}} \mapsto \hat{\mathcal{L}} + \lambda\hat{\mathcal{V}}$, then yield perturbations to the mode frequencies as

$$\delta(-\omega_i^2) \sim \lambda V_{ii} + \lambda^2 \sum_{j\neq i} \frac{|V_{ij}|^2}{\omega_{0,i}^2 - \omega_{0,j}^2} + \mathcal{O}(\lambda^3), \tag{B3}$$

where $V_{ij} = \int d^3r\ \rho\boldsymbol{\xi}_i^* \cdot \hat{\mathcal{V}}\boldsymbol{\xi}_j$ are the matrix elements of the perturbing operator, and the Lagrangian displacement functions are assumed to be unit normalized. For instance, $\hat{\mathcal{V}}$ may be considered to be the difference between the wave operators of two different stellar structures with identical global properties, such that the matrix elements may be expressed as integrals with respect to localized perturbations in the physical quantities of the stellar structure (e.g., the inversion kernels of Kosovichev 1999). In discussions of acoustic glitches, however, one instead supposes that the wave operator $\hat{\mathcal{L}}$ may be notionally decomposed as $\hat{\mathcal{L}}_{\mathrm{smooth}} + \hat{\mathcal{V}}_{\mathrm{sharp}}$. The first term is, in the abstract, the wave operator associated with a "smooth" stellar structure, such that (by assumption) its eigenfunctions are described well by asymptotic approximations such as the JWKB construction, while the second term is associated with localized, sharp, variations in the stellar structure. Because such a decomposition is at best notional, we are free to consider expressions for $\hat{\mathcal{V}}_{\mathrm{sharp}}$ that might otherwise correspond to unphysical structural perturbations in the traditional sense. Moreover, by Equation (B3), we may restrict our attention to the matrix elements of various operators, rather than the operators themselves. In particular, we note that a subset of the terms in Equation (B2), which we shall use to define an operator $\hat{\mathcal{H}}$, have matrix elements

$$\begin{aligned}H_{12} &= \left\langle \boldsymbol{\xi}_1, \frac{1}{\rho}(\nabla(\boldsymbol{\xi}_2\cdot\nabla P) - \boldsymbol{g}\nabla\cdot(\rho\boldsymbol{\xi}_2))\right\rangle \\ &= -\int d^3x\ [\boldsymbol{\xi}_1\cdot\boldsymbol{g}\nabla\cdot(\rho\boldsymbol{\xi}_2) + \boldsymbol{\xi}_2\cdot\boldsymbol{g}\nabla\cdot(\rho\boldsymbol{\xi}_1) \\ &\quad - (\boldsymbol{\xi}_2\cdot\boldsymbol{g})(\boldsymbol{\xi}_1\cdot\nabla\rho)]\end{aligned} \tag{B4}$$

that are Hermitian, by the divergence theorem (and because both $\boldsymbol{g}$ and $\nabla\rho$ point strictly radially). Focusing on the first two terms in particular, the constraints of adiabaticity $\rho' = \frac{P'}{c_s^2} + \rho(\boldsymbol{e}_r\cdot\boldsymbol{\xi})\frac{N^2}{g}$ and of continuity $\rho' = -\nabla\cdot(\rho\boldsymbol{\xi})$ allow us to rewrite this expression as

$$\begin{aligned}\langle\boldsymbol{\xi}_1, \hat{\mathcal{H}}\boldsymbol{\xi}_2\rangle &= \int \rho\ d^3r(-2N^2(\boldsymbol{e}_r\cdot\boldsymbol{\xi}_1)(\boldsymbol{e}_r\cdot\boldsymbol{\xi}_2)) \\ &\quad + (\text{other Hermitian terms}).\end{aligned} \tag{B5}$$

Accordingly, if we were to consider a notional, unphysical decomposition of $\hat{\mathcal{L}}$ as above, in which for $\hat{\mathcal{L}}_{\mathrm{smooth}}$ only this Brunt–Väisälä frequency term were to be modified as $N^2 \mapsto N^2_{\mathrm{smooth}} + \delta N^2$, the corresponding perturbation induced into the mode frequencies, ceteris paribus, would then go as

$$\delta(\omega^2) \sim \langle\boldsymbol{\xi}, \delta\hat{\mathcal{H}}\boldsymbol{\xi}\rangle \sim \int \xi_r^2\cdot\delta N^2\ dm. \tag{B6}$$

More principled decompositions necessarily have a more complicated form. For instance, one might prefer to consider frequency differences arising from more traditional perturbations to the equilibrium ρ, Γ_1, P, etc., in a physically and structurally self-consistent fashion, for which the frequency differences arising from perturbations to specific quantities q are associated with integral kernels of the form

$$V_{ij} = \int(\delta q/q)\ \ K_q[\boldsymbol{\xi}_i, \boldsymbol{\xi}_j]\ dm. \tag{B7}$$

By inspection of Equation (B2), we find these structure kernels, K, must necessarily be bilinear (and therefore quadratic, on the diagonal) in the wave functions of the modes corresponding to each matrix index, or potentially their (anti)derivatives with respect to radial position, as $\hat{\mathcal{V}}$ is permitted to be a general integro-differential operator. Because the asymptotic radial dependence of the (appropriately scaled) wave functions is a power law as $r \to 0$, as we describe above, the overall signature of the near-core feature would then be a linear combination of components, each satisfying a power-law description of the kind we have provided. Our qualitative results would thus not substantially changed were a different quantity to be primarily responsible for producing the acoustic glitch (although each component may have an incremented or decremented power-law index, or a different constant of proportionality).

ORCID iDs

Christopher J. Lindsay https://orcid.org/0000-0001-8722-1436
J. M. Joel Ong https://orcid.org/0000-0001-7664-648X
Sarbani Basu https://orcid.org/0000-0002-6163-3472

References

Arfken, G. B., & Weber, H. J. 2005, Mathematical Methods for Physicists (6th ed.; Amsterdam: Elsevier)
Audard, N., Provost, J., & Christensen-Dalsgaard, J. 1995, A&A, 297, 427
Babikov, V. V. 1976, A Method of Phase Functions in Quantum Mechanics (Moscow: Nauka)
Basu, S., Antia, H. M., & Narasimha, D. 1994, MNRAS, 267, 209
Basu, S., Mazumdar, A., Antia, H. M., & Demarque, P. 2004, MNRAS, 350, 277
Borucki, W. J., Koch, D., Basri, G., et al. 2010, Sci, 327, 977
Brandão, I. M., Cunha, M. S., Creevey, O. L., & Christensen-Dalsgaard, J. 2010, AN, 331, 940
Calogero, F. 1963, NCim, 27, 261
Chaplin, W. J., & Miglio, A. 2013, ARA&A, 51, 353
Corsaro, E., De Ridder, J., & García, R. A. 2015, A&A, 578, A76
Cox, J. P., & Giuli, R. T. 1968, Principles of Stellar Structure (New York: Gordon and Breach)
Cunha, M. S., Avelino, P. P., Christensen-Dalsgaard, J., et al. 2019, MNRAS, 490, 909
Cunha, M. S., & Brandão, I. M. 2011, A&A, 529, A10
Cunha, M. S., & Metcalfe, T. S. 2007, ApJ, 666, 413
Dréau, G., Cunha, M. S., Vrard, M., & Avelino, P. P. 2020, MNRAS, 497, 1008
García, R. A., & Ballot, J. 2019, LRSP, 16, 4
Goldreich, P., & Keeley, D. A. 1977a, ApJ, 211, 934
Goldreich, P., & Keeley, D. A. 1977b, ApJ, 212, 243
Gough, D. O. 1990, in Progress of Seismology of the Sun and Stars, ed. Y. Osaki & H. Shibahashi, Vol. 367 (Berlin: Springer-Verlag), 283
Gough, D. O. 1993, in 47 Session de l'Ecole d'Eté de Physique Théorique: Astrophysical fluid dynamics (Amsterdam: North-Holland), 399
Gough, D. O. 2007, AN, 328, 273
Gough, D. O., & Thompson, M. J. 1988, in IAU Symp. 123, Advances in Helio- and Asteroseismology, ed. J. Christensen-Dalsgaard & S. Frandsen (Dordrecht: Reidel), 155
Grevesse, N., & Sauval, A. J. 1998, SSRv, 85, 161
Hekker, S., & Christensen-Dalsgaard, J. 2017, A&ARv, 25, 1
Houdek, G., & Gough, D. O. 2006, in ESASP 624, Proc. SOHO 18/GONG 2006/HELAS I, Beyond the Spherical Sun, ed. K. Fletcher & M. Thompson (Noordwijk: ESA), 88
Houdek, G., & Gough, D. O. 2007, MNRAS, 375, 861
Kjeldsen, H., & Bedding, T. R. 1995, A&A, 293, 87
Kosovichev, A. G. 1999, JCoAM, 109, 1
Lindsay, C. J., Ong, J. M. J., & Basu, S. 2022, ApJ, 931, 116
Mazumdar, A. 2005, A&A, 441, 1079
Mazumdar, A., & Antia, H. M. 2001, A&A, 377, 192
Mazumdar, A., Basu, S., Collier, B. L., & Demarque, P. 2006, MNRAS, 372, 949
Mazumdar, A., Michel, E., Antia, H. M., & Deheuvels, S. 2012, A&A, 540, A31
Mazumdar, A., Monteiro, M. J. P. F. G., Ballot, J., et al. 2014, ApJ, 782, 18
Miglio, A., Montalbán, J., Carrier, F., et al. 2010, A&A, 520, L6
Monteiro, M. J. P. F. G., Christensen-Dalsgaard, J., & Thompson, M. J. 1998, in IAU Symp. 185, New Eyes to See Inside the Sun and Stars, ed. F.-L. Deubner, J. Christensen-Dalsgaard, & D. Kurtz (Cambridge: Cambridge Univ. Press), 315
Monteiro, M. J. P. F. G., Christensen-Dalsgaard, J., & Thompson, M. J. 2000, MNRAS, 316, 165
Ong, J. M. J., & Basu, S. 2019, ApJ, 885, 26
Ong, J. M. J., & Basu, S. 2020, ApJ, 898, 127
Paxton, B., Bildsten, L., Dotter, A., et al. 2011, ApJS, 192, 3
Paxton, B., Cantiello, M., Arras, P., et al. 2013, ApJS, 208, 4
Paxton, B., Marchant, P., Schwab, J., et al. 2015, ApJS, 220, 15
Paxton, B., Schwab, J., Bauer, E. B., et al. 2018, ApJS, 234, 34
Paxton, B., Smolec, R., Schwab, J., et al. 2019, ApJS, 243, 10
Provost, J., Mosser, B., & Berthomieu, G. 1993, A&A, 274, 595
Reback, J., Mendel, J. B., McKinney, W., et al. 2021, pandas-dev/pandas: Pandas v1.3.0, Zenodo, doi:10.5281/zenodo.3509134
Ricker, G. R., Winn, J. N., Vanderspek, R., et al. 2015, JATIS, 1, 014003
Roxburgh, I. W. 2005, A&A, 434, 665
Roxburgh, I. W. 2010, Ap&SS, 328, 3
Roxburgh, I. W. 2016, A&A, 585, A63
Roxburgh, I. W., & Vorontsov, S. V. 2001, MNRAS, 322, 85
Thoul, A. A., Bahcall, J. N., & Loeb, A. 1994, ApJ, 421, 828
Townsend, R. H. D., & Teitler, S. A. 2013, MNRAS, 435, 3406
Verma, K., Antia, H. M., Basu, S., & Mazumdar, A. 2014, ApJ, 794, 114
Viani, L. S., Basu, S., Ong, J. M. J., Bonaca, A., & Chaplin, W. J. 2018, ApJ, 858, 28
Virtanen, P., Gommers, R., Oliphant, T. E., et al. 2020, NatMe, 17, 261
Vorontsov, S. V. 1988, in ESASP 286, Seismology of the Sun and Sun-like Stars, ed. E. J. Rolfe (Noordwijk: ESA), 475
Vrard, M., Cunha, M. S., Bossini, D., et al. 2022, NatCo, 13, 7553
Vrard, M., Mosser, B., Barban, C., et al. 2015, A&A, 579, A84